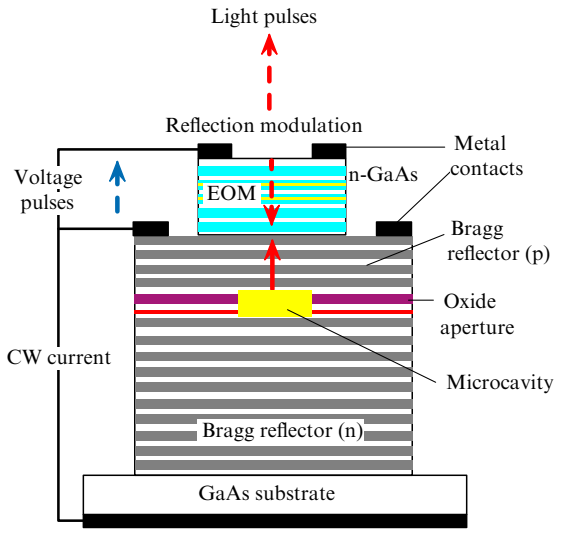

Figure 8. Electrooptically modulated VCSEL. A change in the transmission coefficient of the EOM section in the case of a reverse bias applied to the p–i–n junction in the EOM section having a low capacitance provides ultrahigh operational frequencies of the laser.

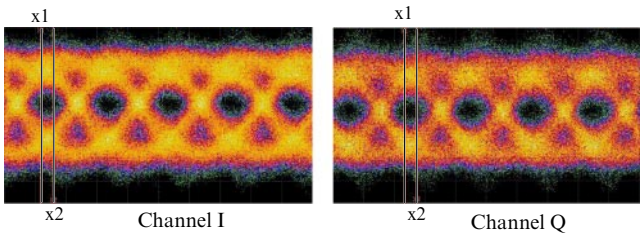

Figure 9. 'Eye diagrams' of an EOM VCSEL obtained in the QPSK multilevel coding mode for a bit rate of 10 Gbit s^{-1} per channel (the total bit rate in the line is 20 Gbit s^{-1}) at a carrier frequency of 13 GHz.

section operating in the reverse bias regime has an extremely low capacitance and can provide operation frequencies equal to 60 GHz [7] and above.

A distinct feature of EOM VCSELs is the high linearity of their characteristics [7], which allows realizing multilevel coding [17]. Figure 9 shows eye diagrams of an EOM VCSEL with the bit rate 10 Gbit s^{-1} per channel (the total bit rate is 20 Gbit s^{-1}) with the use of QPSK coding at the carrier frequency of 13 GHz.

Error-free data transfer was realized at the bit rates up to 16 Gbit s^{-1}. Rapid progress in this field of VCSEL applications can be expected in the near future.

5. Conclusions

Modern VCSELs represent a complex combination of micro- and nanotechnologies. The small size of and low power consumed by the laser in both the current and EOM versions give promise that energy-efficient optical interconnects with bit rates of 50–100 Gbit s^{-1} per channel will be realized and used in new-generation supercomputers, data storage and processing centers, and electronic devices in the consumer market.

The authors thank Zh I Alferov, D Bimberg, S A Blokhin, A E Zhukov, V M Ustinov, and V A Shchukin for the useful discussions. The work was supported by the European Union (grant FP7/2007-2013 according to the VISIT Project Agreement No. 224211) and the Eurostars EC program (the Optical Link Project).

References

1. Benner A "Optical interconnects for HPC", in *Short Distance High Density Optical Interconnects Workshop. An OIDA Roadmapping Workshop, Stanford, CA, April 12–13, 2011*
2. Iga K *IEEE J. Select. Topics Quantum Electron.* **6** 1201 (2000)
3. Alferov Zh I *Fiz. Tekh. Poluprovodn.* **32** 3 (1998) [*Semiconductors* **32** 1 (1998)]
4. Ledentsov N N, Bimberg D, Alferov Zh I *J. Lightwave Technol.* **26** 1540 (2008)
5. Lott J A et al. *Electron. Lett.* **36** 1384 (2000)
6. Tanaka Yu et al. "25 Gbps direct modulation in 1.3-μm InAs/GaAs high-density quantum dot lasers", in *Conf. on Lasers and Electro-Optics, OSA Technical Digest* (Washington, DC: Optical Society of America, 2010) CD, paper CTuZ1
7. Ledentsov N N, Hopfer F, Bimberg D *Proc. IEEE* **95** 1741 (2007)
8. Dingle R, Henry C H "Quantum effects in heterostructure lasers", U.S. Patent No. 3982207, September 21, 1976
9. Ledentsov N N et al. *Proc. SPIE* **7224** 72240P (2009)
10. Bennett A J et al. *Appl. Phys. Lett.* **90** 191911 (2007)
11. Mutig A et al. *Appl. Phys. Lett.* **95** 131101 (2009)
12. Ledentsov N N et al. *Proc. SPIE* **7952** 79520J (2011)
13. Westbergh P et al. *Electron. Lett.* **46** 938 (2010)
14. Hofmann W, Amann M-C *IET Optoelectron.* **2** 134 (2008)
15. Lott J A et al. *Electron. Lett.* **47** 717 (2011)
16. Shchukin V A et al. *Proc. SPIE* **6889** 68890H (2008)
17. Crisp M J et al. *Proc. SPIE* **7933** 79331D (2011)

PACS numbers: **42.65.–k**, **42.70.–a**, **78.67.–n**
DOI: 10.3367/UFNe.0181.201108i.0891

The photonics of self-organizing biomineral nanostructures

Yu N Kulchin

1. Introduction

The possibilities of using optical radiation for the transmission and processing of more and more increasing volumes of information are stimulating the search for principally new technologies aimed at developing the requisite components for communication systems and devices for generating and detecting radiation, and designing optoelectronic computers. Nanophotonic objects such as photonic crystals have been attracting increasing attention recently as promising systems for solving such problems [1]. It is known that Nature has already created various materials with photonic crystal properties, the diversity of these materials including noble opal, the pollen of the butterfly's wing, the beetle's chitin shell, and the mother-of pearl of a shell which grow due to self-organization — one of the most promising technologies. The basic structural components of living systems almost entirely consist of ordered arrays of protein and hydrocarbon molecules. This specific feature of living systems is due to the ability of biological macromolecules to self-organize in

Yu N Kulchin Institute of Automatics and Control Processes, Far-East Branch of the Russian Academy of Sciences, Vladivostok, Russian Federation. E-mail: kulchin@iacp.dvo.ru

Uspekhi Fizicheskikh Nauk **181** (8) 891 – 896 (2011)
DOI: 10.3367/UFNr.0181.201108i.0891
Translated by M Sapozhnikov; edited by A Radzig

solutions [2]. The latter property allows the manufacturing of uniquely intricate nanostructures, providing high efficiency per unit mass without putting in extreme requirements for primary materials and energy. Unfortunately, most natural protein complexes are unstable to temperature variations and chemical actions and can also be easily damaged by bacteria. As a result, direct analogues of biological systems have not found wide applications for manufacturing ordered nanostructures.

At the same time, a rather broad group of biological organisms exists which can concentrate in themselves mineral substances, which are contained in extracellular structures formed by complex composite substances — biominerals. Because they contain two components, organic (proteins or polysaccharides) and mineral (salts or oxides of elements), these self-organizing structures are stable against the action of many environmental factors [2].

A spectacular example of organisms with metabolism based on the self-organizing biomineralization is deep-sea glass sponges (DSGSs), which possess a cellular mechanism of selective accumulation of silicon from water and a complex protein-functioning mechanism, jointly providing the construction of a skeleton system from ordered silicon dioxide nanostructures [2, 3].

In this connection, the study of the morphology and physical and chemical properties of elements of the biomineral skeleton in these objects, in which a mineral component is represented by silicon dioxide, and of the biosilicification process itself in living nature, is of great interest for the development of nanotechnologies.

Along with investigations of biomineralization processes in living nature, researchers in many laboratories are attempting to synthesize biomineral materials with the help of available biopolymers: proteins and polysaccharides. In doing so, biomimetic nanostructured materials are synthesized by sol-gel chemistry methods, which are mainly used in the synthesis of inorganic oxides of silicon, titanium, aluminium, and other chemical elements and are complementary to chemical processes proceeding in living systems.

This paper presents the results of studies on the structure, chemical composition, optical, and nonlinear optical characteristics of DSGS spicules and their artificial biomimetic analogues as new materials for photonics.

2. Morphology and physicochemical characteristics of glass sea sponges

There are about 3000 species of sea sponges, of which about 500 belong to hexacorallia DSGSs [4]. In this paper, we introduce the results of studies of the three types of DSGSs: *Hyalonema sieboldi*, *Pheronema sponge*, and *Sericolophus hawaiicus*, which mainly inhabit the southern seas of the Pacific Ocean. A photograph of a typical sample of sponges of this type is displayed in Fig. 1a. Basal (anchor) spicules of these sponges, which can reach up to 1 m in length, possess an extraordinary elasticity, allowing one to literally knot them (Fig. 1b), whereas skeletal spicules are rather rigid. We selected for studies samples of basal spicules homogeneous over the thickness with lengths from 20 mm to 50 cm and diameters from 40 μm to 1 mm.

A detailed scanning electron microscopic (SEM) study of the transverse sections of basal spicules shows that each of them consists of many axial concentric layers, their number varying from a few dozen to a few hundred, depending on the sponge type and age (Fig. 1c). Each of the concentric layers of a spicule consists of silicon dioxide nanoparticles 20 to 120 nm in size closely packed in a matrix formed by collagen-like nanofibrils and separated between themselves by nanometer protein layers (Fig. 1c) [3, 5, 6]. All the spicules have a central nucleus representing an axial protein filament 1–2 μm in diameter, localized as shown in Fig. 1, and a set of surrounding silicon dioxide and protein component layers [7]. The thickness of layers containing silicon dioxide particles is more than 100 times larger than the thickness of separating protein layers.

Studies performed by the method of energy-dispersive X-ray spectrometry have given evidences that spicules consist mainly of silicon (max $\sim$ 33%), oxygen (max $\sim$ 66%), and carbon (max $\sim$ 9%), with trace amounts of Na and K [8, 9]. It was also established that the chemical composition of the layers is not constant and depends on their location, the sponge shape, and the spicule type.

The study of mechanical characteristics of basal spicules by the method of dynamic ultramicrohardnessmetry [7, 10] have shown that the Young modulus for basal spicules of sea sponges is close to its value for natural opal. It was found that the distribution of the Young modulus over the transverse section of a basal spicule is inhomogeneous and changes from its periphery to center from 33,000 to 40,000 GPa. The

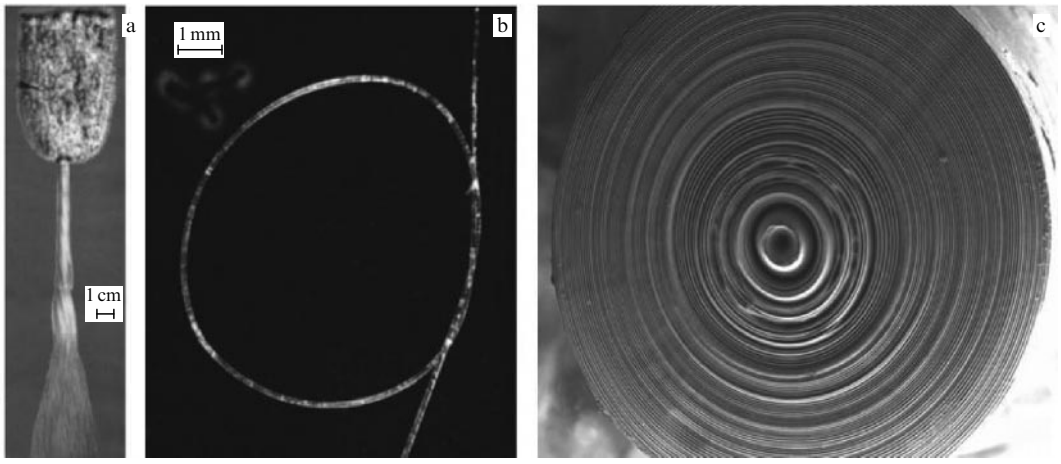

Figure 1. Photographs of *Hyalonema sieboldi* DSGS (a), a fragment of its basal spicule (b), and an SEM photograph of a processed end of a spicule (1157× magnification) (c).

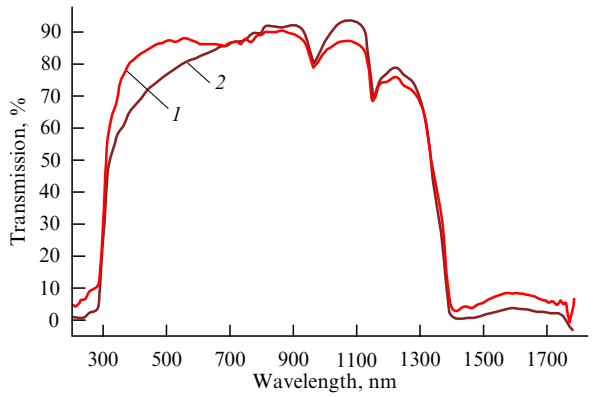

Figure 2. Transmission spectra of *Pheronema raphanus* DSGS spicule materials: curve *1*, basal spicule; curve *2*, skeletal spicule.

mechanical properties of basal spicules observed in experiments are determined by their layered structure and the presence of an organic matrix [3, 9], providing their enhanced mechanical strength and flexibility.

The distribution of the refractive index of a basal spicule over its section measured by the interferometric method [11] demonstrated that the refractive index of layers surrounding the central axial filament is about 1.45–1.48 and decreases to 1.39–1.41 at spicule edges [5, 7], in good agreement with the results reported in paper [11].

The transmission spectrum of the spicule material was recorded in the range from 200 to 1700 nm [9]. Figure 2 demonstrates the transmission spectrum of a *Pheronema raphanus* basal spicule, which is typical for spicules of all types studied here. One can see that the spicule material transmits radiation rather well in the visible and near-infrared spectral ranges. The absorption lines observed at 770, 960, and 1150 nm belong to hydrated silicates contained in spicules, which is consistent with the results obtained in Ref. [11] for basal spicules of a *Hyalonema sieboldi* sponge and other types of sea sponges [3]. The average power loss of the 633-nm laser radiation in the waveguide propagation mode was about 0.1 dB m^{-1} for almost all the spicules studied in our work. The experimental studies of the transverse intensity distribution of radiation propagating in spicules showed that the radiation was concentrated in the axial region ~ 20 μm in size and its spatial distribution was nearly Gaussian [12, 13].

The layered structure of basal spicules also gives rise to the periodic variation of the refractive index over the transverse section on the nano- and micrometer scales. In such a layered structure, the guided radiation modes can propagate with an effective refractive index lower than the refractive index of silicon dioxide. These modes are strongly coupled with light-guiding axial layers. Because of the great difference between the refractive indices of alternating axial layers, the radiation power flux is strongly reflected in the radial direction. In this case, due to a great number of layers in a spicule, for certain values of the effective refractive index of propagating modes the phasing condition can be fulfilled for light fluxes propagating in layers, thereby reducing radiation losses [14].

As shown in papers [12, 15], light can propagate in DSGS spicules only at certain angles to the spicule axis. The resonance wavelength of such a radiation will directly depend on the thickness of layers with a high refractive index. As a result, basal spicules should have forbidden bands, similar to those in photonic crystals. Because the thickness of axial layers with a high refractive index is small, resonance conditions will be fulfilled for the waves propagating at angles close to $\pi/2$ with respect to the normal to the spicule axis. This means that the single-mode propagation regime with the increased size of the mode spot is preferable for radiation guided in basal DSGS spicules. The results of numerical simulations show that this size can reach $\sim 20\,\lambda$ [12]. As the layer thickness is varied from 200 nm to 1 μm, the wavelength resonances of guided radiation will lie in the spectral range from 300 to 1200 nm, in good agreement with experimental findings.

To confirm the presence of photonic crystal properties of basal spicules in glass sea sponges, the propagation of extremely low-energy ≈ 0.01-nJ pulses through them was additionally investigated. Forty-fs, 800-nm pulses were generated by a Ti:sapphire laser at a repetition rate of 1 kHz. The emission spectrum of the laser is presented in Fig. 3a. As expected, the spectra of transmitted radiation for all basal spicules exhibited oscillations. This is illustrated in Fig. 3b by the transmission spectrum of a basal spicule 190 μm in diameter and 40 mm in length, with the central channel ≈ 2 μm in diameter and ≈ 280-nm-thick axial layers with a high refractive index. Experimental studies have given evidences that due to biological growth the thickness of axial layers of basal spicules deviates somewhat from measured average values. Because of this, according to Ref. [14], the maxima of the experimental transmission

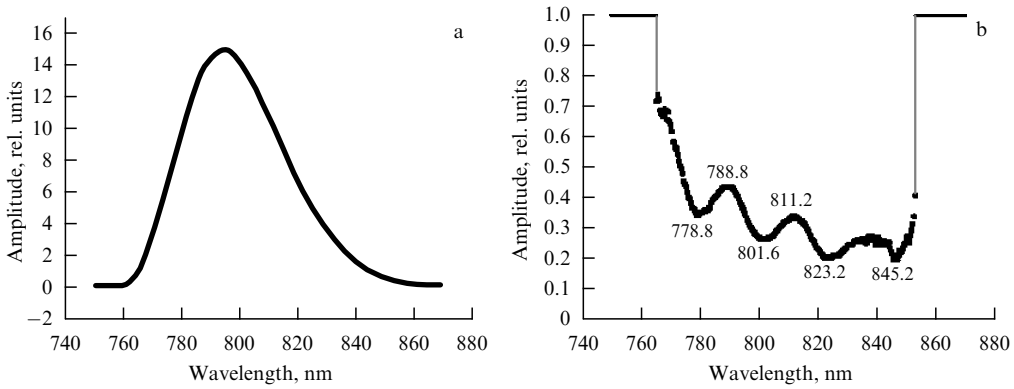

Figure 3. Radiation spectra of ultrashort pulses before (a) and after (b) transmission through a *Hyalonema sieboldi* DSGS spicule (40 mm in length and 190 μm in diameter).

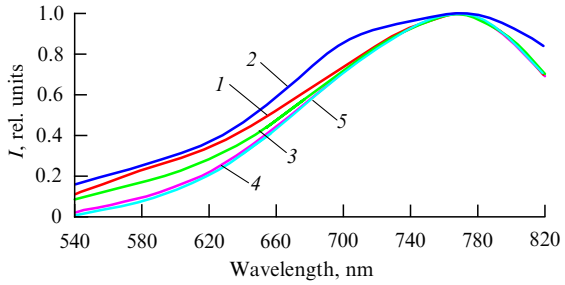

Figure 4. Normalized fluorescence spectra of a *Hyalonema sieboldi* basal spicule at different relative excitation energies of 532-nm, 12-ns input pulses (pulse repetition rate is 10 Hz, the maximum pulse energy is 30 mJ). Attenuation coefficients of the pulse energy are 1 (curve *1*), 0.3 (*2*), 0.2 (*3*), 0.13 (*4*), and 0.1 (*5*).

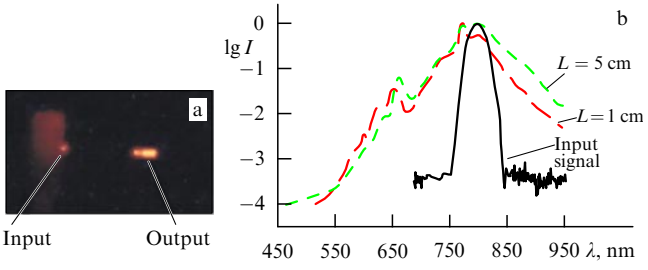

Figure 5. (a) Photograph of supercontinuum generation by 40-fs, 800-nm, 100-nJ ultrashort pulses in a *Hyalonema sieboldi* sponge spicule 200 μm in diameter and 1.5 cm in length. (b) Supercontinuum spectrum after the transmission of pulses through a *Sericolophus hawaiicus* sponge spicule 250 μm in diameter.

spectrum are found to be somewhat smoothed and superimposed on a pedestal, resulting in the comparatively smooth spectrum as a whole.

Thus, the studies have shown that the presence of periodic axial cylindrical silicon dioxide layers in basal DSGS spicules leads to the formation of forbidden photonic bands in them and, therefore, spicules of deep-see glass sponges represent a new type of natural photonic crystals.

3. Nonlinear optical properties of DSGS spicules

Upon excitation of basal spicules by 12-ns, 30-mJ, 532-nm second harmonic pulses from an Nd:YAG laser at a pulse repetition rate of 10 Hz, a considerable increase in the fluorescence intensity in the long-wavelength region was observed [7]. Figure 4 demonstrates the normalized fluorescence spectra of basal spicules 140 μm in diameter and 5 cm in length obtained at different pumping radiation intensities. One can see that the spectra have a maximum in the long-wavelength region at 770 nm, whose position is independent of the laser excitation intensity at the spicule entrance. The spectra differ greatly from the relevant fluorescence spectrum of a usual multimode silica fiber [13]. This is probably explained by the presence of large organic complexes in spicules of glass sea sponges. The measurements of the dependence of the maximum fluorescence intensity at 770 nm on the excitation power showed that this dependence saturated when the excitation power was increased more than 10-fold. This demonstrates the nonlinearity of the light-energy transformation in spicules related to a high concentration of organic complexes inhomogeneously distributed in them [16]. A specific feature of glass sea sponges is their fluorescence lifetime. The fluorescence lifetime of basal spicules measured at different excitation powers reaches a few dozen microseconds, considerably exceeding these lifetimes, for example, for sea zooplankton or quartz optical fibers ($\approx 10^{-10}-10^{-9}$ s) [17].

A unique property of glass sea spicules as optical fibers with a periodically changing transverse distribution of the refractive index is the complicated frequency profile of the dispersion for light pulses propagating in them, which substantially differs from analogous profile for conventional optical fibers. As a result, new nonlinear-optical phenomena and new regimes of spectral–temporal transformation of ultrashort light pulses can be observed in such 'optical fibers'.

In this connection, a model was constructed to describe the propagation of ultrashort pulses in spicules taking into account the combined action of dispersion effects, nonlinear polarization, and ionization nonlinearity leading to the self-phase modulation of the light field and efficient transformation of the pulse spectrum to a supercontinuum; in addition, the propagation of ultrashort pulses in DSGS spicules was numerically simulated and studied experimentally [18]. Experiments were performed using a Spitfire Pro Ti:sapphire laser complex (Spectra Physics, USA) emitting $\approx$ 0.9-mJ, 40-fs, $\approx$ 800-nm single pulses at a pulse repetition rate of 100 Hz with a spectral FWHM of 35 nm.

On coupling $\approx$ 5-nJ ultrashort pulses into different DSGS spicules 5–15 mm in length, the self-focusing of radiation was observed with the formation of 'hot regions' in the transverse intensity distribution of transmitted light beams. The shape of emission spectra in these regions noticeably changed [19]. The nonlinear-optical coefficient of the spicule material measured in the self-focusing of ultrashort pulses in spicules was $n_2 \approx 8.8 \times 10^{-16}$ cm^2 W^{-1}, which exceeds this coefficient for silica by more than three times, and by approximately 10^3 times for air.

As the laser pulse energy was increased above $\approx$ 20 nJ, the stable formation of a supercontinuum was observed in the spectrum of radiation transmitted through spicules, while prolonged repeated irradiation by 0.1–0.9-mJ pulses caused the optical breakdown of the spicule material. Figure 5a displays a photograph illustrating the transformation of the spectrum of a 100-nJ femtosecond pulse transmitted through a *Hyalonema sieboldi* sponge spicule 200 μm in diameter and 1.5 cm in length to a supercontinuum covering the visible spectrum down to 400 nm. Figure 5b shows that the observed spectrum of ultrashort pulses transmitted through a spicule considerably broadens upon increasing the spicule length.

Because the peak intensity of unfocused ultrashort pulses could achieve $\approx 7 \times 10^{10}$ W cm^{-2} in experiments, this resulted in the considerable enhancement of nonstationary processes such as transient spatial self-focusing and multiphoton ionization of the spicule material, and the short-wavelength edge of the supercontinuum shifted to 300 nm as the spicule length increased.

The simulation of the intensity spectral distribution of ultrashort light pulses in the 750–850-nm region transmitted through a spicule and its comparison with experimental data showed that the group velocity dispersion $\beta_2 = 2.8 \times 10^{-3}$ ps^2 m^{-1} for spicules is an order of magnitude lower than this dispersion in similar silica fibers, which is explained by the significant contribution from the wave-

guide part of dispersion due to the multilayer quasiperiodic structure of the cladding [15] compared to the contribution from the component caused by the spicule material.

4. Biosilicate nanocomposite materials and their nonlinear-optical properties

As mentioned in the Introduction, inorganic oxides are mainly synthesized by sol-gel chemistry methods [20]. Their synthesis is performed, as a rule, by using the two-stage introduction of biopolymers into a silicate matrix at the sol-gel transition stage; this process does not cause the mineralization of biomacromolecules. In Refs [19, 21], a new, one-stage method was proposed for the synthesis of biomimetic hybrid nanocomposite materials based on a silicon-containing tetraxis (2-hydroxyethyl) orthosilicate precursor (THEOS) (50%) and Na alginate (0.5–1%), Na hyaluronate (0.1–2%), and xanthane (0.5–2%) polysaccharides. This method does not involve the stage of sol solution formation that takes place in the conventional two-stage process.

In this case, the structure of the inorganic component of the nanocomposite material being produced is determined by a polysaccharide organic matrix, similarly to the formation of inorganic compounds in living organisms occurring due to their precipitation (biomineralization) on biomacromolecules serving as templates. In this connection, the mechanism of formation of such biosilicates resembles one of the mechanisms used by Nature for the synthesis of spicules.

By proceeding this process at a low temperature, we fabricated the samples of transparent biosilicate materials with transmission in the spectral range from 350 to 1400 nm virtually the same as that of the DSGS spicule material [19]. The refractive index of the synthesized materials was $n = 1.517$. The organic macromolecules contained in small concentrations in these materials play the role of a morphological matrix in the form of intricately intersected fibrils penetrating the entire material (Fig. 6a). The rest of the material volume is filled with spherical silicate particles (with an average diameter of 60 nm) deposited onto the organic matrix. Figure 6b gives a photograph of a transparent nanocomposite synthesized in an aqueous solution containing 50% of the THEOS precursor and 1% of sodium hyaluronate. The sample length is 15 mm [19].

The study of the interaction of unfocused ≈ 1-mJ femtosecond laser pulses (the laser beam diameter was 7 mm, and pulse repetition rate 100 Hz) with synthesized nanocomposite biomimetic media revealed that the nonlinear-optical parameters of these media were considerably higher than those for DSGS spicules [19]. The spectra of ultrashort pulses transmitted through xanthane, Na-alginate, and Na hyaluronate composite samples 10 mm in length demonstrate that the nonlinearity of the interaction of intense ultrashort pulses with these materials manifests itself much stronger (Fig. 6c). Here, the self-phase modulation of pulses caused by the Kerr nonlinearity of a medium and the self-focusing of pulses play the main role, which, together with other nonlinear-optical processes, leads to the formation of filaments in samples (Fig. 6b) and a supercontinuum. The best conversion efficiency of the pulse energy to a supercontinuum was achieved in sodium hyaluronate samples, for which higher energy levels were observed in supercontinuum spectrum (Fig. 6c). Sodium alginate samples proved to be optically unstable, while xanthane samples strongly absorbed ultrashort laser pulses.

A comparison of total supercontinuum energies P_{SC} generated in the spectral range from 400 to 650 nm in samples with the same geometry and different bioorganic additions (up to 1% in weight) revealed that P_{SC} for sodium hyaluronate samples was more than twice the P_{SC} for xanthane samples. The stable generation of a supercontinuum was observed in sodium hyaluronate samples even with a thickness as small as 1 mm. The approximate estimate of the nonlinear-optical coefficient of the sodium hyaluronate material based on the experimental study of the filamentation process in samples and data in paper [19] gives the value of $n_2 \approx 29 \times 10^{-14}$ cm^2 W^{-1}, which exceeds this coefficient for the DSGS spicule material by more than two orders of magnitude.

Another important feature of the supercontinuum generation in this material relates to the dependence of the total supercontinuum power P_{SC} on the concentration of

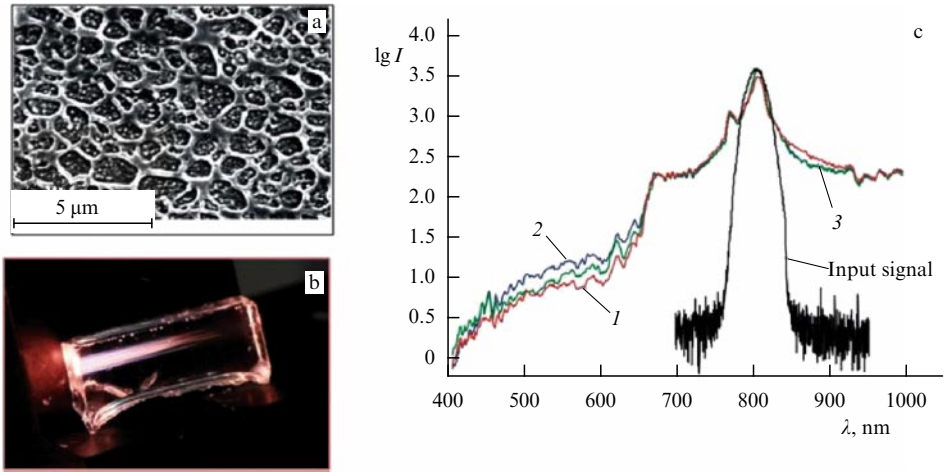

Figure 6. (a) SEM photograph of a section of an Na hyaluronate nanocomposite sample. (b) Photograph of an Na hyaluronate nanocomposite sample and a filament produced in it. (c) Supercontinuum spectra generated in nanocomposite materials based on the following complexes: THEOS (50%) + xanthane (0.5%) (curve *1*); THEOS (50%) + Na hyaluronate (0.25%) (curve *2*), and THEOS (50%) + Na alginate (0.25%) (curve *3*).

sodium hyaluronate polysaccharide and sample length [19], which allows one to control the nonlinear-optical parameters of the material itself and functional elements based on it.

5. Conclusion

The studies considered above have shown that the combination of proteins and polysaccharides created by Nature and self-organized with silicon dioxide extracted from sea water under natural conditions produced a unique nonlinear-optical biomineral nanocomposite material combining the flexibility and strength of a protein with the elasticity and strength of silicon dioxide, which is promising for applications in photonics. This process can be reproduced under artificial conditions using the adaptable sol-gel technology, which opens up a broad perspective for manufacturing new passive and active optoelectronic devices.

References

1. Churyumov G I, Maksimov I S, Ust'yantsev M A *Usp. Sovrem. Radioelektron.* (11) 35 (2005)
2. Meyers M A et al. *Prog. Mater. Sci.* **53** 1 (2008)
3. Müller W E G et al. *Biosensors Bioelectron.* **21** 1149 (2006)
4. Leys S P, Mackie G O, Reiswig H M *Adv. Marine Biol.* **52** 1 (2007)
5. Kulchin Yu N et al. *Vestn. Dal'nevost. Otd. Ross. Akad. Nauk* (1) 27 (2007)
6. Kulchin Yu N et al. *Opt. Memory Neural Networks* **16** 189 (2007)
7. Kulchin Yu N et al. *Kvantovaya Elektron.* **38** 51 (2008) [*Quantum Electron.* **38** 51 (2008)]
8. Galkina A N et al. *Khim. Fiz. Mezoskop.* **11** 310 (2009)
9. Voznesenskii S S et al. *Ross. Nanotekhnol.* **5** (1–2) 126 (2010) [*Nanotechnol. Russia* **5** (1–2) 142 (2010)]
10. Kulchin Yu N *Rare Met.* **28** (Special issue) 66 (2009)
11. Aizenberg J et al. *Proc. Natl. Acad. Sci. USA* **101** 3358 (2004)
12. Kul'chin Yu N et al. *Pis'ma Zh. Tekh. Fiz.* **34** (15) 1 (2008) [*Tech. Phys. Lett.* **34** 633 (2008)]
13. Kulchin Yu N et al. *Fotonika Biomineral'nykh i Biomimeticheskikh Struktur i Materialov* (Photonics of Biomineral and Biomimetic Structures and Materials) (Moscow: Fizmatlit, 2011)
14. Konorov S O et al. *Zh. Eksp. Teor. Fiz.* **123** 975 (2003) [*JETP* **96** 857 (2003)]
15. Kul'chin Yu N et al. *Opt. Spektrosk.* **107** 468 (2009) [*Opt. Spectrosc.* **107** 442 (2009)]
16. Maslov D V, Ostroumov E E, Fadeev V V *Kvantovaya Elektron.* **36** 163 (2006) [*Quantum Electron.* **36** 163 (2006)]
17. Agrawal G P *Nonlinear Fiber Optics* (San Diego: Academic Press, 1995) [Translated into Russian (Moscow: Mir, 1996)]
18. Kulchin Yu N et al., in *Biosilica in Evolution, Morphogenesis, and Nanobiotechnology* (Eds W E G Müller, M A Grachev) (Berlin: Springer, 2009) p. 315
19. Kulchin Yu N et al. *Laser Phys.* **21** 630 (2011)
20. Dunn B et al. *Acta Mater.* **46** 737 (1998)
21. Shchipunov Yu A, in *Perspektivnye Napravleniya Razvitiya Nanotekhnologii v DVO RAN* (Promising Directions in the Development of Nanotechnologies at the Far Eastern Branch, Russian Academy of Sciences) Vol. 2 (Executive Ed. Yu N Kulchin) (Vladivostok: Dal'nauka, 2009) p. 157

PACS numbers: 37.10.De, 37.10.Gh, 32.30.Jc
DOI: 10.3367/UFNe.0181.201108j.0896

Laser cooling of rare-earth atoms and precision measurements

N N Kolachevsky

1. Introduction

Today, the physics of microwave and optical frequency standards is one of the most rapidly advancing lines of inquiry. Progress here can be readily quantitatively evaluated: while in the early 2000s the problem of reaching a measurement inaccuracy at a level of 10^{-15} was considered [1], now systems capable of generating highly stable signals with a fractional inaccuracy better than 10^{-17} are being developed [2].

The improvement in frequency stability opens new possibilities for solving problems of time and frequency metrology, global positioning and navigation, geodesy, gravimetry, and the sensitive testing of fundamental physical theories. The solution to these problems at the modern level of precision requires the practical realization of new principles of generating time and frequency signals on Earth surface and in space. In 2014, the orbital launching of ACES (Atomic Clock Ensemble in Space) is planned, which constitutes an ensemble of high-precision microwave atomic clocks with an inaccuracy of a few digits in the 16th decimal place [3]. Simultaneously, methods are being developed for transmitting extremely stable signals via both conventional microwave channels and optical communication lines [4]. Precise time and frequency signals are required in numerous fundamental and applied problems, making this research field one of the most urgent issues in modern physics.

A considerable improvement in the accuracy of frequency standards has been achieved mainly due to advances in the development of optical clocks operating in the frequency range close to $\nu_0 \sim 10^{15}$ Hz. The increase in the carrier frequency compared to microwave standards ($\nu_0 \sim 10^{10}$ Hz) for the same spectral linewidth $\delta\nu$ has led to an increase in the resonance quality factor $Q = \nu_0/\delta\nu$ and a corresponding decrease in the inaccuracy. To excite and detect narrow optical transitions (the typical width today is $\delta\nu \sim 1$ Hz), it is necessary to solve a number of problems: (i) to create stable laser systems emitting lines with spectral widths smaller than 1 Hz; (ii) to search for optimal atomic and ion systems providing the best metrological characteristics, and (iii) to develop methods for cooling atoms and for exciting and interrogating resonances providing the ultimate accuracy.

Recent advances in the stabilization of lasers have proved to be so significant (see review [5]) that these light sources have become a reliable tool accessible to any laboratory in the

N N Kolachevsky Lebedev Physical Institute, Russian Academy of Sciences, Moscow, Russian Federation;
Moscow Institute of Physics and Technology (State University), Dolgoprudnyi, Moscow region, Russian Federation
E-mail: kolik@lebedev.ru

Uspekhi Fizicheskikh Nauk **181** (8) 896 – 903 (2011)
DOI: 10.3367/UFNr.0181.201108j.0896
Translated by M Sapozhnikov; edited by A Radzig